IEEE Photonics Journal
An IEEE Photonics Society Publication

Open Access

High Sensitivity of Refractive Index Sensor Based on Analyte-Filled Photonic Crystal Fiber With Surface Plasmon Resonance

Volume 7, Number 3, June 2015

Zhenkai Fan
Shuguang Li
Qiang Liu
Guowen An
Hailiang Chen, Student Member, IEEE
Jianshe Li
Dou Chao
Hui Li
Jianchen Zi
Wenlong Tian

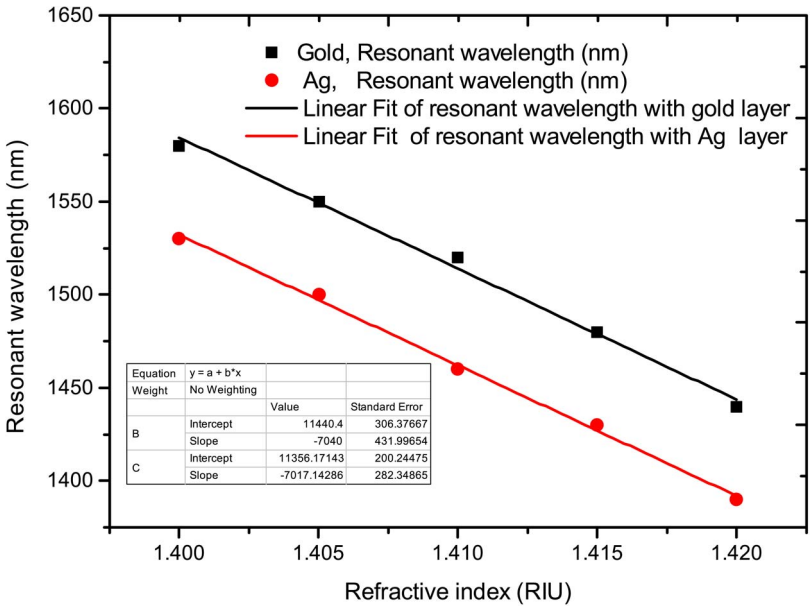

DOI: 10.1109/JPHOT.2015.2432079
1943-0655 © 2015 IEEE

High Sensitivity of Refractive Index Sensor Based on Analyte-Filled Photonic Crystal Fiber With Surface Plasmon Resonance

Zhenkai Fan,[1,2] Shuguang Li,[1] Qiang Liu,[1] Guowen An,[1] Hailiang Chen,[1] *Student Member, IEEE*, Jianshe Li,[1] Dou Chao,[1] Hui Li,[1] Jianchen Zi,[1] and Wenlong Tian[2]

[1]Key Laboratory of Metastable Materials Science and Technology, College of Science, Yanshan University, Qinhuangdao 066004, China
[2]Laboratory of Optical Physics, Beijing National Laboratory for Condensed Matter Physics, Institute of Physics, Chinese Academy of Sciences, Beijing 100190, China

DOI: 10.1109/JPHOT.2015.2432079

Manuscript received February 11, 2015; revised May 4, 2015; accepted May 6, 2015. Date of publication May 12, 2015; date of current version June 10, 2015. This work was supported in part by the National Science Foundation (NSF) through the NSF ERC Center for Extreme Ultraviolet Science and Technology under NSF Award EEC-0310717, by the National Natural Science Foundation of China under Grants 61178026 and 61475134, and by the Natural Science Foundation of Hebei Province, China, under Grant E2012203035. Corresponding author: S. Li (e-mail: shuguangli@ysu.edu.cn).

Abstract: Two kinds of novel plasmonic high sensitivity of refractive index (RI) sensors based on analyte-filled photonic crystal fiber (AF-PCF) are proposed in this paper. The metallic gold and silver is used as the surface plasmon resonance activity metal. A full-vector finite-element method is applied to analyze and investigate the sensing and coupling characteristics of this designed AF-PCF with the gold or silver layer. Phase matching between the second surface plasmon polariton and fundamental modes can be met at different wavelengths as the analyte of the RI is increased from 1.40 to 1.42. The phase-matching wavelength of the designed AF-PCF with the gold layer is shifted to the longer wavelength direction compared with that with the silver layer, and the resonance strength is much stronger. The average sensitivities of 7040 and 7017 nm/RIU in the sensing are arranged from 1.40 to 1.42 with high linearity are achieved for the designed sensors with the gold and silver layers, respectively, which are almost the same. However, the figure of merit with the silver layer is much better than that with the gold layer.

Index Terms: Photonic crystal fiber, surface plasmon resonance (SPR), refractive index sensor.

1. Introduction

Surface plasmon resonance (SPR) technology as an method for measuring the refractive index (RI) has attached continuous research interests in chemical and biosensing [1]–[3], as the high sensitivity to RI change of the surrounding medium. SPP are excitations on the metal dielectric surface which is impassioned by the coupling of an electromagnetic field into the charge-density oscillations on the metal surface [4], [5]. To implement SPR sensing, one prerequisite is to meet the phase match condition between the SPP mode and the core mode at a given wavelength [6]. With the variation of liquid-analyte RI, the phase matching between the SPP mode and the core mode can be met in different wavelengths where the resonance leak of loss can occur. Over the past few decades, various types of microstructure fiber-based refractive index sensor

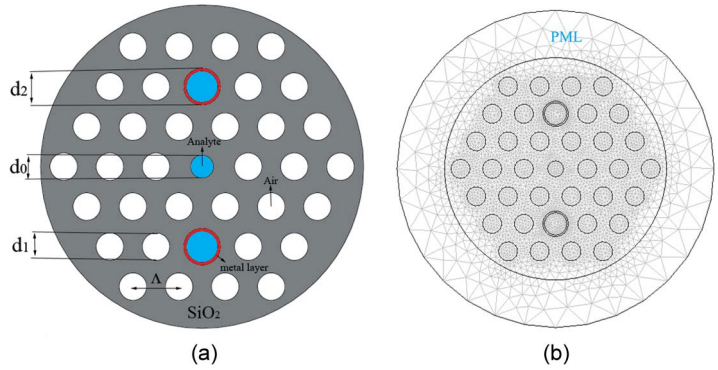

Fig. 1. (a) Cross section of the designed SPR sensors with the gold and silver layers. The metal layer represents the gold or Ag. (b) FEM mesh and scattering boundary condition for computation.

have been demonstrated based on the surface plasmon resonance. Erdmanis *et al.* [7] present and numerical characterize a surface plasmon resonance sensor based on an H-shaped PCF with the sensitivity of 5000 nm/RIU. Lee *et al.* [8] reported a novel RI sensor based on a polymer microstructure fiber directional coupler for low index sensing whose sensitivity can reach to 1400 nm/RIU. Coelho *et al.* [9] proposed a sensing structure based on SPR in chemically etched single mode optical fiber. The sensitivity of 3800 and 5100 nm/RIU were obtained for the reflection and for the transmission mode, respectively.

Furthermore, photonic crystal fiber, owning to a flexible array of air holes along the propagation direction, provides an attractive platform to implement the phase matching for the SPR sensing. Tan *et al.* designed a novel fiber SPR sensor based on a hollow core PCF with the liquid-mixture filled in the core whose sensitivity can exceed the 6430 nm/RIU for an aqueous environment [9]. Hao *et al.* in 2013 reported a SPR RI sensor based on an active Yb^{3+}-doped PCF [10]. The sensitivity can be influenced obviously by slight change of the RI of liquid analyte in the air holes. Besides, Yu *et al.* [11] proposed a selectively coated PCF based on SPR sensor. Its good sensitivity as high as 5500 nm/ RIU can be achieved in the designed PCF.

In this paper, we report two kinds of novel high sensitivity of sensors based on analyte-filled photonic crystal fiber with the gold or silver layer and present a comprehensive numerical characterization based on the finite element method. The complete coupling pays a crucial role in SPR sensing system, which has been analyzed by using the coupled-mode theory. As the phase matching between second-order SPP mode and fundamental mode is met, the energy of fundamental mode will be coupled to the surface of metal layer at the given wavelength where the loss spectrum between the second-order SPP mode and the fundamental mode can occur avoided crossing point. However, the phase matching conditions of the designed AF-PCF with gold layer and the designed AF-PCF with silver layer can be satisfied in different wavelengths, the resonance strength in the gold surface is much stronger than that in the surface of silver layer. The avoided crossing point can be influenced obviously by a bit change of RI of liquid analyte in the air holes of PCF, which has a promising future in RI of sensor. Numerical simulation demonstrates that the sensitivities of two kinds of sensors can reach to 7040 and 7017 nm/RIU in the sensing arrange from 1.40$\sim$1.42, and a high linearity can be achieved.

2. The Novel Structure and Principle of SPR Sensors

The cross section of the designed SPR sensors with gold and sliver layers are shown in Fig. 1(a), which can be acquired by the perfectly developed stack-and-draw fabrication process. The designed AF-PCF is composed of three layer of air holes arranged with a regular triangular lattice. The lattice constant of Λ is 2 μm. The liquid analyte is infiltrated into the center small air channel, which forms the fiber-core of the designed AF-PCF. Two large air holes around the fiber-core are plated a-40 nm- thickness of gold or silver layer whose remaining blue air channel is also infiltrated into the liquid analyte. Besides, the diameter of blue channel of d_0 is 0.5 μm,

the diameter of white air hole of d_1 is 0.6 μm, and the diameter of large air hole with the metal layer of d_2 is 0.8 μm. RI of liquid analyte is changed from 1.40 to 1.42, and RI of air is set as 1. As shown in Fig. 1(b), the FEM mesh is used to discrete the physical field for calculation. The outermost boundary of this AF-PCF is assigned with scattering boundary condition. Liu *et al.* [12] in 2015 designed two kinds of polarization filter based on photonic crystal fiber with nano-scale gold film. The differences between two metal layers and a metal layer included in this design are analyzed in detail. It reveals that the loss with two metal layers at the resonance wavelength is greatly increased than that with one metal layer, while the resonance wavelength with two metal layers in the designed AF-PCF is not shifted compared with that with one metal layer. A perfectly matched layer (PML) with several micrometers is added to the outmost layer, which is used to absorb the radiation power.

In this designed sensing structure is focused two important advantages. First of all, it increases to the sensitivity for the high refractive index of the liquid, as the central liquid channel is introduced. Second, as the designed AF-PCF is simple and symmetrical, we can easily draw after drawing tower by a suitable temperature. Next, we are able to coat the metal film in the designed AF-PCF by the gas-phase condensation method because of this gold lower boiling point than the melting point of silicon glass. The background material is pure silica, whose material dispersion can be calculated by the Sellmeier equation [13]

$$n(\lambda) = \sqrt{1 + \frac{B_1{}^2}{\lambda^2 - C_1} + \frac{B_2{}^2}{\lambda^2 - C_2} + \frac{B_3{}^2}{\lambda^2 - C_3}} \tag{1}$$

where $B_1 = 0.691663$, $B_2 = 0.407943$, $B_3 = 0.897479$, $C_1 = 0.004679$, $C_2 = 0.013512$, and $C_3 = 97.934003$. λ is the wavelength of free space. In our paper, the sensing properties of the designed sensors coated gold and silver layers are researched by the FEM at the same time. As the dielectric properties of the gold and silver are different, the phase matching conditions of coated gold and silver can be satisfied at different wavelengths. Next, the permittivity of the gold layer can be approximated by using the Drude–Lorentz model, as [14]

$$\varepsilon_m = \varepsilon_\infty - \frac{\omega_D^2}{\omega(\omega + j\gamma_D)} - \frac{\Delta\varepsilon \cdot \Omega_L^2}{(\omega^2 - \Omega_L^2) - j\Gamma_L\omega} \tag{2}$$

where the values and physical meaning of ε_∞, ω_D, γ_D, Ω_L, and Γ_L can be read in [15]. Furthermore, the permittivity of the silver layer in the designed AF-PCF is simulated by using the Drude–Lorentz model with five Lorentz oscillators, as [16]

$$\varepsilon = \varepsilon_1 - \frac{\omega_p^2}{\omega(\omega + i\gamma_p)} - \sum_{m=1}^{5} \frac{f_m \cdot \omega_m^2}{\omega_m^2 - \omega^2 - i\gamma_m\omega} \tag{3}$$

where the parameters of ε_1, ω_p, ω_m, f_m,γ_m and the damping rate γ_p can be read in [17]. In the (2) and (3), the refractive indexes of the second order-SPP modes of gold and silver in the AF-PCF can be obtained by solving the permittivities of gold and silver.

3. Numerical Result and Analysis

Coupled-mode theory (CMT) plays a crucial role in the refractive index of SPR sensor in the AF-PCF. Coupling characteristics of the second SPP mode and the fundamental mode can be simulated when a beam of broadband light is launched into the designed AF-PCF with gold or silver layer. At the phase matching wavelength, the resonance strength of the fundamental mode and the second-order SPP mode is the strongest. For two coupled modes, the rigorous derivation of CMT is expressed by using the coupled equations [18]

$$\begin{cases} \frac{dH_1}{dZ} = i\beta_1 H_1 + i\kappa H_2 \\ \frac{dH_2}{dZ} = i\beta_2 H_1 + i\kappa H_2 \end{cases} \tag{4}$$

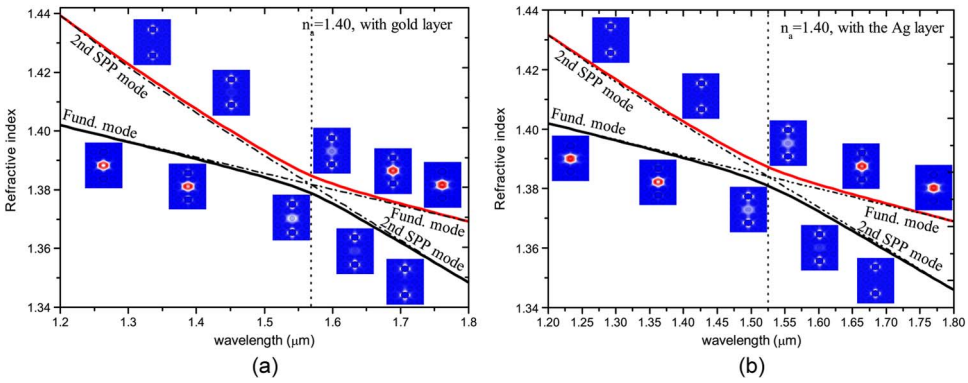

Fig. 2. (a) Wavelength dependance on the dispersion relations of the fundamental mode and the second-order SPP mode in this designed AF-PCF with the gold layer. (b) Wavelength dependance on the dispersion relations of the fundamental mode and the second-order SPP mode in this designed AF-PCF with the silver layer. The analyte RI of n_a is equal to 1.40. (Inserts) Electric field distributions of two coupled modes at a specific wavelength.

where H_1 and H_2 are two coupling mode fields of the fundamental mode and the second order SPP mode, respectively. β_1 and β_2 are their propagation constants, and κ is the coupling strength. Assume that $H_1 = A_1\exp(i\beta z)$ and $H_2 = A_2\exp(i\beta z)$, and the propagation constant of coupling mode β can be calculated

$$\beta_{\pm} = \beta_{\text{ave}} \pm \sqrt{\delta^2 + \kappa^2} \tag{5}$$

where $\beta_{\text{ave}} = (\beta_1 + \beta_2)/2$ and $\delta = (\beta_1 - \beta_2)/2$. For the fundamental mode and the second SPP mode, β_1 and β_2 are extremely complex. Here, δ is also complex, which can be defined as $\delta = \delta_r + i\delta_i$. According to this derivation, the real parts of two coupled mode of propagation constants are equal at the phase matching wavelength. Furthermore, when $\delta_r = 0$, it can be derived that $\delta^2 + \kappa^2 = -\delta_i^2 + \kappa^2$. When $\delta_i < \kappa$, (β_+) and (β_-) have different real parts but equal imaginary parts. A complete coupling (regular anti-crossing) between a fundamental mode and second order SPP mode occurs. On the other hand, when $\delta_i > \kappa$, (β_+) and (β_-) have identical real part while different imaginary part and an incomplete coupling happens.

Then we numerically simulate the coupled-mode process between the fundamental mode and the second SPP mode in this designed AF-PCF with the gold or silver layer, which is obviously observed in Fig. 2. When the refractive index crossing between the fundamental mode and the second SPP mode, the real parts of the effective refractive indexes of the fundamental mode and second SPP mode are equal, where the incomplete coupling can be obtained. Conversely, when the refractive index anti crossing between the fundamental mode and second SPP mode, the imaginary parts of the effective indexes of the fundamental mode and second SPP mode are equal, where the complete coupling can be achieved. As shown in Fig. 2(a), the dispersion relations of the fundamental mode and the second SPP mode can avoid crossing at the phase matching wavelength, when the refractive index of n_a is 1.40 for the designed AF-PCF with the gold layer. We can see that the phase matching condition can be met at the given wavelength of 1.57 μm while the refractive indexes of the fundamental mode and the second SPP mode is never equal. The inserts in Fig. 2(a) illustrate the powers of the fundamental mode and the second SPP mode can be transformed into each other. At the shorter wavelength, the energy of the fundamental mode is mainly limited to the fiber-core, with the increasing of the wavelength, the energy of the fundamental mode is gradual transferred into the second SPP mode. For the second SPP mode, at shorter wavelength, the energy is completely coupled into the fundamental mode at longer wavelength. In the avoided crossing point, the electric fields of fundamental mode and second SPP mode are almost identical in order that it is difficult to distinguish them. For this designed AF-PCF with the silver layer from Fig. 2(b), the dispersion relationships of the

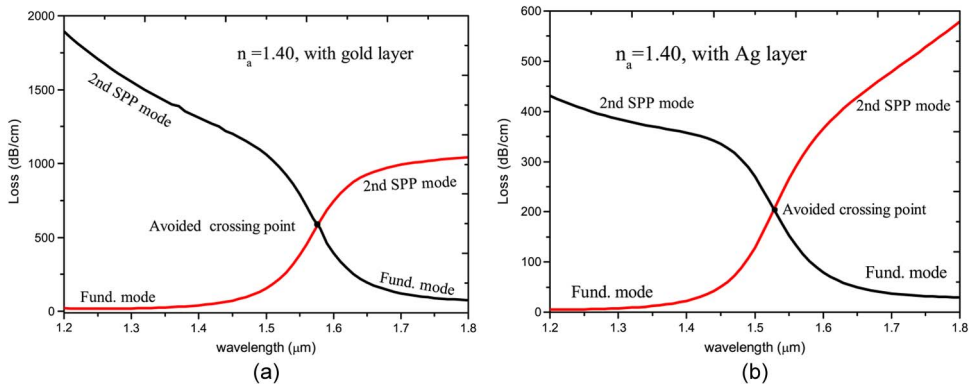

Fig. 3. (a) Wavelength dependance on the confine loss of the core mode and the second-order SPP mode in the AF-PCF with gold layer. (b) Wavelength dependance on the confine loss of the core mode and the second-order SPP mode in the AF-PCF with silver layer. The RI of n_a is 1.40.

fundamental mode and the second SPP mode is never crossing at phase matching wavelength. It is obvious that the coupled-mode process of the fundamental mode and the second SPP mode of the AF-PCF with the silver layer is closely analogous compared to the designed AF-PCF with gold layer, while the avoided crossing wavelengths are different. Thus, the phase matching between the fundamental mode and the second SPP mode is satisfied in the shorter wavelength compared with that of the designed AF-PCF with gold layer when the RI of n_a is 1.40.

At phase matching wavelength, resonance coupling between the fundamental mode and the second-order SPP mode can be well achieved, the confine loss of the fundamental mode can reach the strongest. In the designed AF-PCF with metal layer, the spectrum of modal loss plays a crucial role in terms of the SPR sensor, which can be defined as [19]

$$L = 8.686 \times \frac{2\pi}{\lambda} Im[n_{\text{eff}}] \times 10^4 \tag{6}$$

where λ represents the operating wavelength, $Im[n_{\text{eff}}]$ is the imaginary part of the RI. As shown in Fig. 3(a), we can see that the completely energy transfer can be understood from the loss spectrums of the fundamental mode and the second SPP mode in this designed AF-PCF with the gold layer. At the avoided crossing wavelength, as the imaginary parts of the fundamental mode and the second SPP mode is equal, the completely coupling between the fundamental mode and the second SPP mode can be obtained, the modal loss of the fundamental mode reach to the largest, the modal loss of the second SPP mode is the smallest. The loss of the fundamental mode at the shorter wavelength can transfer into the second SPP mode after passing through the phase matching wavelength, from Fig. 3(a), which can be shown in red line. For the black line, it is opposite that the modal loss transferring is from the second SPP mode to the fundamental mode. It is obviously observed from Fig. 3(b) that the completely loss conversion process between the fundamental mode and the second SPP mode is almost similar in this designed AF-PCF with the silver layer compared to the AF-PCF with the gold layer. Furthermore, the resonance strength between the fundamental mode and the second SPP mode in this designed AF-PCF with the gold layer is much stronger than that in the designed AF-PCF with the silver layer when the designed structure parameters of AF-PCF with the gold and silver layers and the liquid analyte RI of n_a are same. As the dielectric constants of gold and the silver are different, the phase matching between the fundamental mode and the second SPP mode in this designed AF-PCF with the gold and silver layers can occur in different wavelengths.

As the liquid-analyte RI in this designed AF-PCF is different, the phase matching between the fundamental mode and the second SPP mode can be met in different wavelengths, which can be used as the RI of sensor. The loss spectrums of the fundamental modes of the designed AF-PCF with the gold layer are presented in Fig. 4(a). When the liquid analyte of RI is

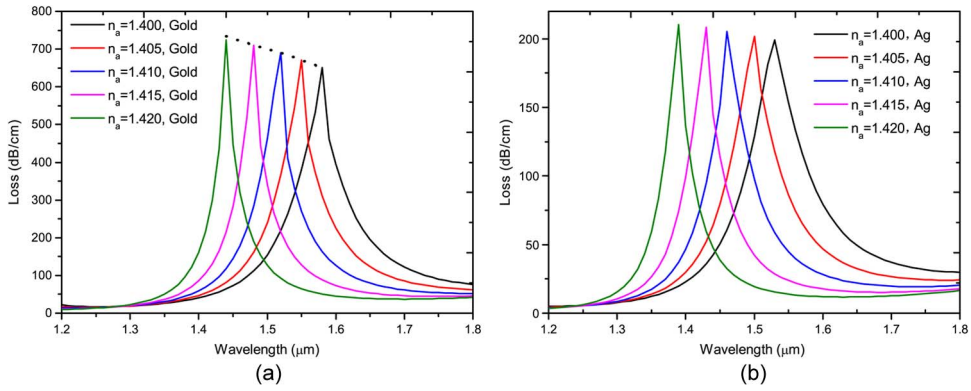

Fig. 4. (a) Wavelength dependance on the confine losses of different liquid analytes in this designed AF-PCF with the gold layer. (b) Wavelength dependance on the confine losses of different liquid analytes in this designed AF-PCF with the silver layer.

increased from 1.40 to 1.42, a step growth of 0.005, the loss peak of the fundamental mode is shifted from the wavelength 1.58 μm to the wavelength 1.44 μm, and the value of loss peak is increasing from the 650.9 dB/cm to 733.8 dB/cm. For the metal silver, the loss spectrum of shifting rule is the same as the increasing of the RI of liquid analyte in this designed AF-PCF. As shown in Fig. 4(b), we can see that the loss spectrum of the designed AF-PCF with the silver layer vary with the change of RI of liquid analyte from 1.40 to 1.42, the loss peak of the fundamental mode is shifted from the wavelength 1.53 to 1.39. Compared with the designed AF-PCF with the gold layer, the loss spectrums of the designed AF-PCF with the silver layer is moved toward the shorter wavelength direction as a whole. The values of loss peaks are increased from the 199 dB/cm to the 210 dB/cm. We can find the resonance strength between the fundamental mode and the second-order SPP mode for the AF-PCF with the gold layer is much stronger than that for the designed AF-PCF with silver layer. The full width at half-maximum (FWHM) of the loss spectrums are gradually narrowed in different RI of n_a.

In this part, we analyze the sensitivity of the designed AF-PCF with the gold or silver layer on the RI change of liquid analyte. The sensitivity of SPR-based RI of sensor is defined by the resonance wavelength dependance on the unit analyte RI change, which is given in units of nm/RIU. In this simulation, an average sensitivity within a given analyte RI range is achieved by only measuring multiple sets of resonance wavelength and the RI of n_a. The resonance wavelength with respect to the RI of liquid analyte shows a nonlinear feature in the designed AF-PCF with gold or silver layer, while the scattering points of the designed AF-PCF with gold layer own a larger slope compared to the designed AF-PCF with the silver layer. In the same analyte RI, it is easy to rationalize that the resonance wavelength of the designed AF-PCF with the gold layer is shifted to the longer wavelength direction compared to the designed AF-PCF with the silver lay. The corresponding linear fitting line of the sensitivity of the designed AF-PCF with gold or silver layer are presented in Fig. 5. The linear-fitting equations are

$$\lambda_{\text{gold}} = -7040n + 11\,440, \qquad 1.40 \le n_a \le 1.42 \tag{7}$$

$$\lambda_{\text{silver}} = -7017n + 11\,356, \qquad 1.40 \le n_a \le 1.42 \tag{8}$$

where λ_{gold} and λ_{silver} are the two resonance wavelengths of the liquid analyte in this designed AF-PCF with the gold and silver layers, respectively. n represents the RI of testing sample. The slopes of the two equations give two average RI sensitivities of the liquid analyte. Two averages sensitivities of 7040 and 7017 nm/RIU can be achieved in the relevant sensing range of 1.40 $\sim$ 1.42. The significance of PCF structure helps in attaining the high sensitivity sensing. Two large air holes and central air holes can easily be infiltrated into more analyte liquid. The refractive index of fundamental mode can be influenced by the analyte liquid. Thus, the phase matching wavelength can be efficiently shifted with the increasing of the liquid refractive index.

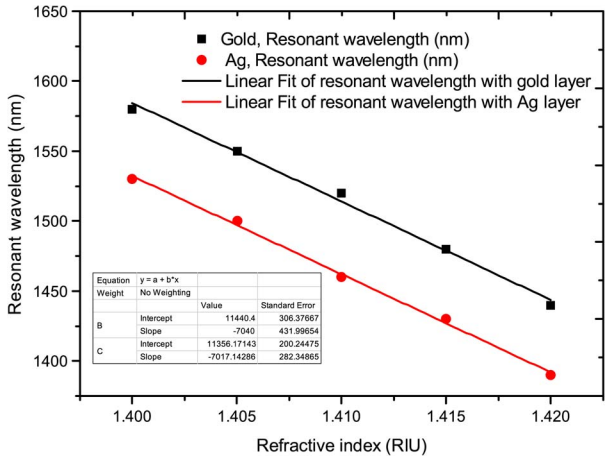

Fig. 5. Linear fitting lines of the resonant wavelength versus analyte of RI in this designed AF-PCF with the gold layer or silver layer.

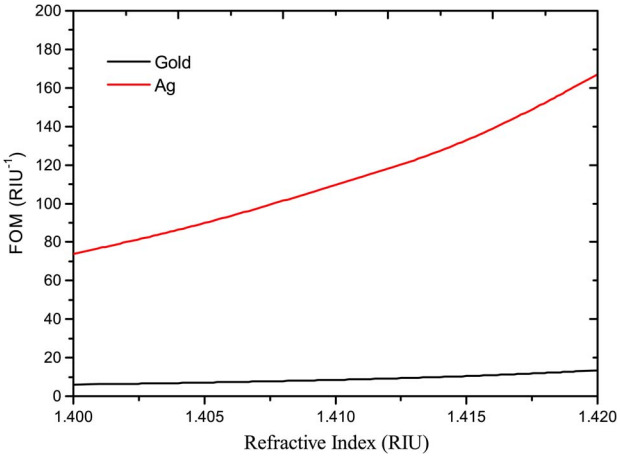

Fig. 6. Variation of the FOM and analyte RI in the designed AF-PCF with gold or silver layer.

It can be seen that the SPRs achieved the metal gold and silver on the sensitivity of liquid analyte are almost same. The high sensitivities and linearities make them possible to work as two calibration sensors.

The signal to noise ratio (SNR) is an important parameter for the improved design. It is well known that the larger SNR will lead to a much more reduced standard deviation of the spectral variation. Furthermore, the improvements in spectral width and SNR can promote to a better detection limit for the RI sensor, which can demonstrated by using the figure of merit (FOM). The FOM is defined by [4], [20]

$$\text{FOM} = \frac{S\ (\text{nm/RIU})}{\text{FWHM}\ (\text{nm})} \tag{9}$$

where S is the linear slop of the resonance wavelength dependance on the refractive index and FWHM is the full width at half-maximum. In this simulation, the FOM of the designed AF-PCF with gold or silver layer is shown in Fig. 6. It is seen that the FOM of the designed AF-PCF with the silver layer is much higher compared to the designed AF-PCF with a gold layer. The FOM of the designed AF-PCF with the silver layer is rapidly rising with the increasing of the liquid analyte of refractive index. However, the FOM curve is very flat for the designed AF-PCF with the

gold layer. The FOM values of the designed AF-PCF with the gold or silver layer can reach to 73.8 and 5.9 RIU^{-1} at 1.40 RIU. Compared with the designed AF-PCF with the gold layer, the designed AF-PCF with the silver layer is more suitable to be applied for the RI sensor.

However, this probe can be not used to sense refractive index around 1.330 as the designed AF-PCF structure is quite insensitive to the lower refractive index of liquid analyte. There are two mainly reasons. Firstly, the area of the central air channel is accounted for most of fiber core. The low refractive index liquid analyte is infiltrated into the central air channel, which greatly reduces the fiber core of refractive index, which eventually leads to the fiber-core refractive index close to the cladding refractive index. Then, the energy will be difficult to be limited in fiber-core. Second, from the experimental point of view, the lower refractive index liquid is infiltrated into the central air channel, while the energy is difficult to couple into the fiber-core.

4. Conclusion

We designed two kinds of novel high-sensitivity RI of sensors based on AF-PCF with the gold or silver layer in this paper, which is based on coupled-mode theory. The sensing and coupled-mode properties of this designed AF-PCF with the gold or silver layer is analyzed and investigated by using the finite element method. As phase matching between the fundamental mode and the second SPP mode can be met at the avoided crossing point, the complete resonance coupling between the fundamental mode and the second SPP mode can be achieved. The resonance wavelength of the fundamental mode and the second SPP mode can be obviously shifted with a slight change of liquid analyte RI. The average sensitivities of 7040 and 7017 nm/RIU in the sensing range of $1.40 \sim 1.42$ can be achieved for the designed AF-PCF with the gold and silver layers, which show the high linearity feature. In short, the designed AF-PCF with the silver is more suitable to be used as the SPR-based RI sensor since the FOM of the designed AF-PCF with the silver layer is much higher than that with the gold layer and their sensitivities are also almost identical.

References

[1] R. Otupiri *et al.*, "A novel birefrigent photonic crystal fiber surface plasmon resonance biosensor," *IEEE Photon. J.*, vol. 6, no. 4, Aug. 2014, Art. ID. 6801711.
[2] J. Zhou *et al.*, "Intensity modulated refractive index sensor based on optical fiber Michelson interferometer," *Sens. Actuators B, Chem.*, vol. 208, pp. 315–319. Nov. 2014.
[3] E. Akowuah, T. Gorman, S. Haxha, and J. V. Oliver, "Dual channel planar waveguide surface plasmon resonance biosensor for an aqueous environment," *Opt. Exp.*, vol. 18, no. 24, pp. 24 412–24 422. Nov. 2010.
[4] J. Narayan Dash and R. Jha, "Graphene-based birefringent photonic crystal fiber sensor using surface plasmon resonance," *IEEE, Photon. Technol. Lett.*, vol. 26, no. 11, pp. 1092–1095. Nov. 2014.
[5] B. Liu, Y. Jiang, X. Zhu, X. Tang, and Y. Shi, "Hollow fiber surface plasmon resonance sensor for the detection of liquid with high refractive index," *Opt. Exp.*, vol. 21, no. 26, pp. 32 349–32 357. Dec. 2013.
[6] Y. Du, S. Li, and S. Liu, "Wavelength-selective characteristics of high birefringence photonic crystal fiber with Au nanowires selectively filled in the cladding air holes," *Chin. Phys. B*, vol. 21, no. 9, Feb. 2012, Art. ID. 094219.
[7] M. Erdmanis *et al.*, "Comprehensive numerical analysis of a surface plasmon resonance sensor based on an H-shaped optical fiber," *Opt. Exp.*, vol. 19, no. 15, pp. 13 980–13 988, Jul. 2011
[8] K. Lee *et al.*, "Refractive index sensor based on a polymer fiber directional coupler for low index sensing," *Opt. Exp.*, vol. 22, no. 14, pp. 17 497–17 507, Jul. 2014.
[9] Z. Tan *et al.*, "Sensing structure based on surface plasmon resonance in chemically etched single mode optical fibres," *Plasmonics*, vol. 9, no. 1, pp. 167–173, Sep. 2014.
[10] C. J. Hao *et al.*, "Surface plasmon resonance refractive index sensor based on active photonic crystal fiber," *IEEE Photon. J.*, vol. 5, no. 6, Dec. 2013, Art. ID. 4801108.
[11] X. Yu *et al.*, "A selectively coated photonic crystal fiber based surface plasmon resonance sensor," *J. Opt.*, vol. 12, no. 1, Dec. 2010, Art. ID. 015005.
[12] Q. Liu, S. Li, and H. Chen, "Two kinds of polarization filter based on photonic crystal fiber with nanoscale gold film" *IEEE Photon. J.*, vol. 7, no. 1, Feb. 2015, Art. ID. 2700210.
[13] E. Akowuah *et al.*, "Numerical analysis of a photonic crystal fiber for biosensing applications," *IEEE J. Quantum Elect.*, vol. 48, no. 11, pp. 1403–1410, Nov. 2012.
[14] H. Lee, M. Schmidt, H. Tyagi, L. Sempere, and P. Russell, "Polarization-dependent coupling to plasmon modes on submicron gold wire in photonic crystal fiber," *Appl. Phys. Lett.*, vol. 93, no. 11, Sep. 2008, Art. ID. 111102.
[15] W. Chen, M. Thoreson, S. Ishii, A. Kildishev and V. Shalaev, "Ultra-thin ultra-smooth and low-loss silver films on a germanium wetting layer," *Opt. Exp.*, vol. 18, no. 5, pp. 5124–5134, Mar. 2010.

[16] Z. Zhang, Y. Shi, B. Bian, and J. Lu, "Dependence of leaky mode coupling on loss in photonic crystal fiber with hybrid cladding,"*Opt. Exp.*, vol. 16, no. 3, pp. 1915–1922, Feb. 2008.
[17] J. Xue *et al.*, "Polarization filter characters of the gold-coated and the liquid filled photonic crystal fiber based on surface plasmon resonance," *Opt. Exp.*, vol. 21, no. 11, pp. 13 773–13 740, May 2013.
[18] L. Sherry *et al.*, "Localized surface plasmon resonance spectroscopy of single silver nanocubes," *Nano Lett.*, vol. 5, no. 10, pp. 2034–2038, Aug. 2005.
[19] J. Dash and R. Jha, "On the performance of graphene-based D-shaped photonic crystal fibre biosensor using surface plasmon resonance," *Plasmonics*, pp. 1–9, Feb. 2015. DOI: 10.1007/s11468-015-9912-7.
[20] Z. Zhang, Y. Tsuji, and M. Eguchi, "Design of polarization splitter with single-polarized elliptical-hole core circular-hole holey fibers," *IEEE Photon. Technol. Lett.*, vol. 26, no. 6, pp. 541–543, Mar. 2014.